

Design Considerations for 2D Dirac-Source FETs: Device Parameters, Non-Idealities and Benchmarking

Peng Wu, *Member, IEEE*, and Joerg Appenzeller, *Fellow, IEEE*

Abstract—Dirac-source field-effect transistors (DS-FETs) have been proposed as promising candidates for low-power switching devices by leveraging the Dirac cone of graphene as a low-pass energy filter. In particular, using two-dimensional (2D) materials as the channel in a DS-FET is of interest for ultimate scaling purposes. In this paper, we investigate the design considerations for 2D DS-FETs using ballistic simulations based on Landauer formalism. We study the impact of several key device parameters on the device performance, such as graphene doping, Schottky barrier heights, and effective mass of the 2D channel. In addition, we study the impact of non-idealities on the performance of DS-FETs, such as graphene disorder and rethermalization, as well as ways to mitigate them. Finally, we benchmark the performance of DS-FETs for different channel materials, providing a guide for the proper choice of material for 2D DS-FETs.

Index Terms—Low-power, steep-slope, Dirac-source field-effect transistor (DS-FET), 2D materials, graphene, MoS₂, Schottky barrier, effective mass, disorder, rethermalization.

I. INTRODUCTION

SCALING down the supply voltage (V_{DD}) is critical for reducing the power consumption of transistors and integrated circuits (ICs). However, the subthreshold swing (SS) of conventional MOSFETs is fundamentally limited to ~ 60 mV/dec at room temperature, which hinders the reduction of V_{DD} , while maintaining a low off-state current (I_{OFF}). To overcome the SS limit, several novel device concepts have been proposed, such as tunnel field-effect transistors (TFETs) [1]–[5], negative-capacitance FETs (NC-FETs) [6], [7], nanoelectromechanical (NEM) relays [8] and impact-ionization MOS (IMOS) [9], [10]. In particular, Dirac-source field-effect transistors (DS-FETs) have been recently proposed and demonstrated as a promising candidate [11], [12]. DS-FETs leverage the Dirac cone of graphene as a low-pass energy filter

Manuscript received XXXX, 2022; This work was supported by Intel Corporation.

Peng Wu was with the School of Electrical and Computer Engineering, Purdue University, West Lafayette, IN 47907 USA, and also with the Birck Nanotechnology Center, Purdue University, West Lafayette, IN 47907 USA. He is now with the Research Laboratory of Electronics, Massachusetts Institute of Technology, Cambridge, MA 02139 USA (e-mail: wu936@alumni.purdue.edu).

Joerg Appenzeller is with the School of Electrical and Computer Engineering, Purdue University, West Lafayette, IN 47907 USA, and also with the Birck Nanotechnology Center, Purdue University, West Lafayette, IN 47907 USA.

to enable a “cold electron source”, thus achieving a steep slope at room-temperature. Unlike TFETs, in which the transmission of band-to-band tunneling (BTBT) limits the on-state current I_{ON} , a DS-FET does not suffer from this limitation and has the potential of achieving a large I_{ON} alongside with a steep slope.

The first demonstration of a DS-FET had been based on a carbon nanotube (CNT) as channel material [11]. However, there has also been interest in building DS-FETs using two-dimensional (2D) materials, such as molybdenum disulfide (MoS₂) [12]–[14], since the atomically thin body thicknesses of 2D materials allow for ultimate scaling of device dimensions. Moreover, integration becomes easier for 2D channels than individual 1D tubes. In this paper, we study the design considerations for 2D DS-FETs.

The paper is organized as follows. In Section II, we study the basic operation principles of 2D DS-FETs. In Section III, we discuss the impact of device parameters on the performance of 2D DS-FETs as well as the impact of non-idealities, based on ballistic simulations using Landauer formalism. Finally, in Section IV, we benchmark different channel materials for 2D DS-FETs, before concluding in Section V.

II. BASIC OPERATION PRINCIPLES

In this section, we discuss the basic operation principles of 2D DS-FETs. Without loss of generality, we discuss n-type DS-FETs in this paper and the discussions apply to p-type DS-FETs by reversing the doping type of the graphene Dirac source (from p-type to n-type) and the polarities of gate and drain biases (from positive to negative), as well as by replacing the transport parameters (effective mass and valley degeneracy) of electrons with those of holes.

Fig. 1(a) and Fig. 1(b) show the schematic and band diagram of a 2D DS-FET. The device is composed of a graphene source, a 2D semiconductor channel (2DSC), source (S) and drain (D) contacts, a control gate (CG) that controls the doping in the graphene Dirac source, and a gate (G) that controls the channel as well as a segment of the graphene that makes contact to the 2DSC. For the n-type DS-FET under study, the graphene Dirac source is p-doped, while the graphene segment in contact with the 2DSC channel is n-doped by the gate G in the on-state to lower the Schottky barrier height to the 2DSC [15]–[18]. Note that the band movement of the graphene segment under control of G has not been depicted in Fig. 1(b) for simplicity, which we will reevaluate later in the manuscript. The basic operation of a 2D DS-FET can be understood from the Landauer formula [19]–[21]:

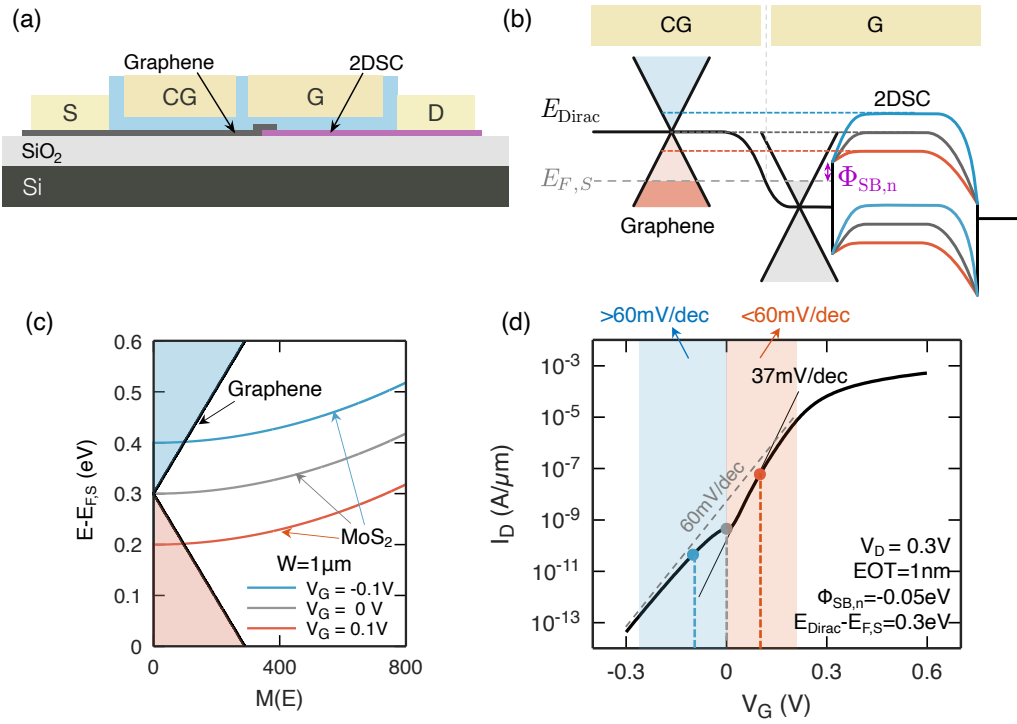


Fig. 1. Basic operation principle of a 2D DS-FET. (a) Schematic of a 2D DS-FET. (b) Band diagram of a 2D DS-FET at different gate voltages applied to G. (c) Number of modes of the graphene source and the MoS₂ channel at different gate voltages. (d) Simulated transfer characteristics of an MoS₂ DS-FET.

$$I = \frac{2q}{h} \int M(E)T(E)[f(E - E_{F,S}) - f(E - E_{F,D})]dE \quad (1)$$

where $T(E)$ is the transmission probability, f is the Fermi-Dirac distribution function, and $M(E)$ is number of modes, which is determined by the smaller one of i) $M(E)$ in the graphene source and ii) $M(E)$ in the 2DSC channel, given by:

$$M_{Gr}(E) = W \frac{2|E - E_{Dirac}|}{\pi \hbar v_F} \quad (2)$$

$$M_{2DSC}(E) = W g_C \frac{\sqrt{2m_e^*(E - E_C)}}{\pi \hbar} \quad (3)$$

where $W = 1 \mu\text{m}$ is the device width, $v_F = 10^6 \text{ m/s}$ is the Fermi velocity of graphene, E_{Dirac} is the energy at the Dirac point in the graphene source, g_C is the conduction band valley degeneracy of the 2DSC, m_e^* is the electron effective mass of the 2DSC, and E_C is the conduction band minimum of the 2DSC channel. As an example, Fig. 1(c) shows the number of modes of the graphene source and the 2DSC channel, in this case, an MoS₂ channel ($m_e^* = 0.51 m_0$, $g_C = 2$ [22]). In general, the graphene source has a smaller $M(E)$ than the MoS₂ channel for energy levels above E_C of MoS₂ (except very close to E_C). Therefore, $M(E)$ in the Landauer formula (1) is determined by $M_{Gr}(E)$, while the MoS₂ channel behaves as a gate-tunable energy barrier that blocks the current below E_C (here we ignore any ambipolar hole injection from the drain side due to a large bandgap of 1.8 eV of monolayer MoS₂ [23]). If we also assume that $T(E) = 1$ for $E > E_C$ (i.e. we ignore scattering in the MoS₂ channel and assume perfect transmissions for the Klein tunneling in the graphene p-n junction [24], [25] and at the graphene-MoS₂ contact) and that the drain voltage is large enough so that $f(E - E_{F,D}) \approx 0$ within the energy range of interest

($E > E_C$), we can rewrite (1) as:

$$I = \frac{2q}{h} \int_{E_C}^{\infty} M_{Gr}(E) f(E - E_{F,S}) dE \quad (4)$$

Note that $M_{Gr}(E)$ in the Dirac source is independent of gate voltage. Therefore, we can treat $M_{Gr}(E) \times f(E - E_{F,S})$ as an effective distribution function, and thus $M_{Gr}(E)$ filters the Fermi-Dirac tail and modulates the SS of the DS-FET. Since $f \approx \exp[-(E - E_{F,S})/k_B T]$ (for $E - E_{F,S} \gg k_B T$, where k_B is Boltzmann constant, $T = 300 \text{ K}$ is temperature) is a fast-decaying exponential function, a small energy range of $\sim k_B T$ above E_C contributes to most of the current I in eq. (4) in the off-state of the DS-FET ($E_C - E_{F,S} \gg k_B T$). Therefore, $M_{Gr}(E)$ near E_C of the channel determines the SS of the device. As indicated by the orange lines in Fig. 1(b) and Fig. 1(c), if E_C of MoS₂ aligns with the lower cone of the graphene source, $M_{Gr}(E)$ decreases with increasing energy and the effective distribution function $M_{Gr}(E) \times f(E - E_{F,S})$ is a super-exponential decaying function with energy E , thus the graphene source acts as a low-pass energy filter and enables a sub-60 mV/dec switching. However, if E_C of MoS₂ crosses the Dirac point and reaches the upper cone of the graphene source, indicated by the blue lines in Fig. 1(b) and Fig. 1(c), $M_{Gr}(E)$ increases with increasing energy, and thus the graphene source acts as a high-pass filter and the SS becomes larger than 60 mV/dec. The high-pass filtering above the Dirac point has a strong impact on the device characteristics and should not be ignored [13], [14] when analyzing DS-FET operation.

Next, we simulate the transfer characteristics of an MoS₂ DS-FET based on Landauer formula (1). In the simulation, we have considered the quantum capacitance C_q [26] of MoS₂ to calculate the band movement of E_C with gate voltage V_G :

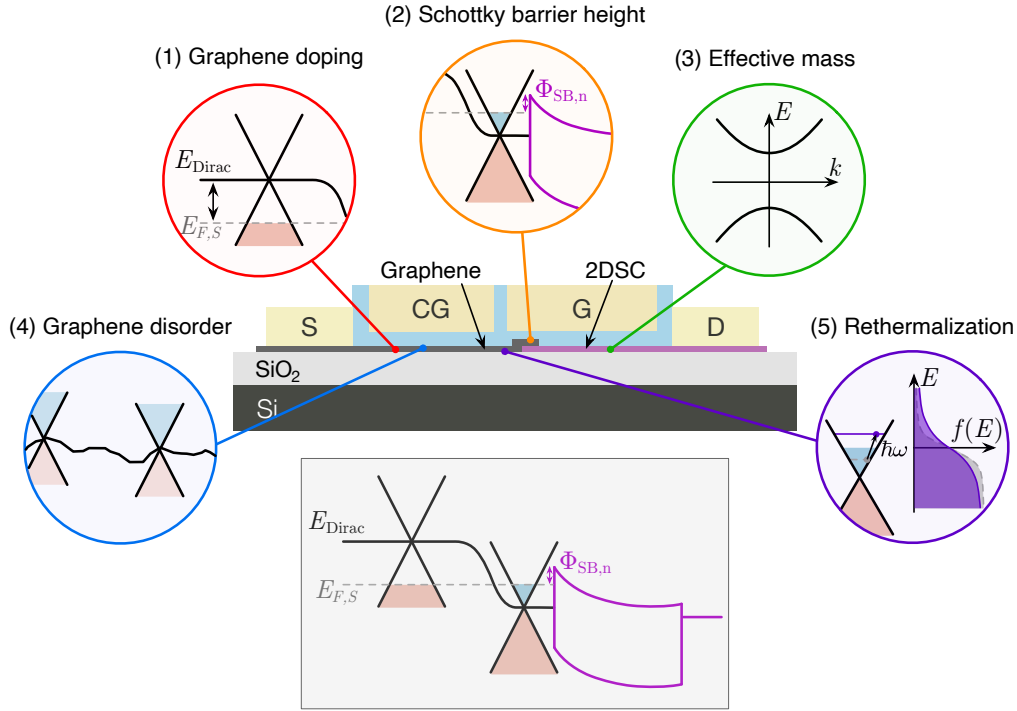


Fig. 2. Design considerations for 2D DS-FETs, including device parameters: (1) graphene doping; (2) Schottky barrier height; (3) effective mass; and non-ideal effects: (4) graphene disorder; (5) rethermalization.

$$\frac{d\psi_S}{dV_G} = \frac{d(-E_C/q)}{dV_G} = \frac{C_{ox}}{C_{ox} + C_q} \quad (5)$$

where ψ_S is channel potential, C_{ox} is gate oxide capacitance (we assume an EOT of 1 nm for the gate oxide). The quantum capacitance C_q is given by:

$$C_q = q^2 \frac{1}{2} D_{2D} f(E_C - E_{F,S}) = q^2 \frac{1}{2} \frac{g_C m_e^*}{\pi \hbar^2} \frac{1}{1 + \exp\left(\frac{E_C - E_{F,S}}{k_B T}\right)} \quad (6)$$

where $D_{2D} = g_C m_e^* / \pi \hbar^2$ is the 2D density of states (DOS) of the MoS₂ channel, which is a constant value irrespective of energy in a 2D system, and the prefactor 1/2 accounts for the fact that only the positive velocity states are filled at large drain biases in a ballistic transistor [27]. We also set $E_C - E_{F,S} = 0.3$ V at $V_G = 0$ V as the origin for the band movement. Combined with eqs. (5) and (6), we can determine a one-to-one mapping between V_G and E_C . Fig. 1(d) shows the simulated $I_D - V_G$ transfer characteristics of an MoS₂ DS-FET. One can see that the DS-FET reaches an SS of 37 mV/dec, thanks to the aforementioned low-pass filtering effect. The SS value is in agreement with a previous simulation study on 2D MoS₂ DS-FETs [12]. In addition, as indicated by the grey dot in Fig. 1(d), a kink can be observed in the $I_D - V_G$ curve at $V_G = 0$ V, which separates the region with SS below 60 mV/dec [orange shaded region in Fig. 1(d)] and the region with SS above 60 mV/dec [blue shaded region in Fig. 1(d)]. The kink corresponds to where the E_C of MoS₂ crosses the Dirac point of the graphene source, indicated by the dashed grey line in Fig. 1(b), which is in agreement with our previous discussion on the change from low-pass filtering below the Dirac point to high-pass filtering above the Dirac point. Such kink is a signature of DS-FET, and its existence can be used to validate the DS-FET operation. Also note that the steepest slope is located right above the kink in the $I_D - V_G$ curve, corresponding to when the E_C of MoS₂ channel

is just below the Dirac point in the graphene source. This is because $M_{Gr}(E)$ is approaching zero close to the Dirac point and thus gives rise to the strongest low-pass filtering effect.

III. DEVICE PARAMETERS AND NON-IDEALITIES

In this section, we discuss the impact of device parameters and non-idealities on the performance of 2D DS-FET. We discuss the following devices parameters: (1) graphene doping; (2) Schottky barrier height; (3) effective mass; and the following non-ideal effects: (4) graphene disorder; (5) rethermalization, as shown in Fig. 2.

A. Graphene Doping

In the previous section, we have shown that the steepest slope occurs just above the kink in the $I_D - V_G$ curve, which corresponds to the situation when the E_C of MoS₂ is just below the Dirac point energy E_{Dirac} of the graphene source, as shown in Figs. 1(b-d). By tuning the doping levels in the graphene Dirac source using the control gate (CG), one can tune the energetic difference between E_{Dirac} and the source Fermi level $E_{F,S}$ and change the band position of E_C (and thus the V_G and I_D) at which the steepest slope is achieved.

Fig. 3 shows the simulated transfer characteristics of an MoS₂ DS-FET with different doping levels in the graphene Dirac source, expressed as $E_{Dirac} - E_{F,S}$. One can see that with a higher doping level, the position of the kink in the $I_D - V_G$ characteristics shifts to a more negative V_G and a smaller I_D . Since the SS is not constant and has an abrupt change at the kink, rather than comparing the steepest SS at one point, a more appropriate way to evaluate the performance is to compare the ΔV_G (i.e. the V_G sweep range) needed for the same I_{OFF} and I_{ON} (e.g., 1 nA/ μ m and 10 μ A/ μ m, respectively). For a too high doping level ($E_{Dirac} - E_{F,S} = 0.4$ eV, blue line in Fig. 3), the

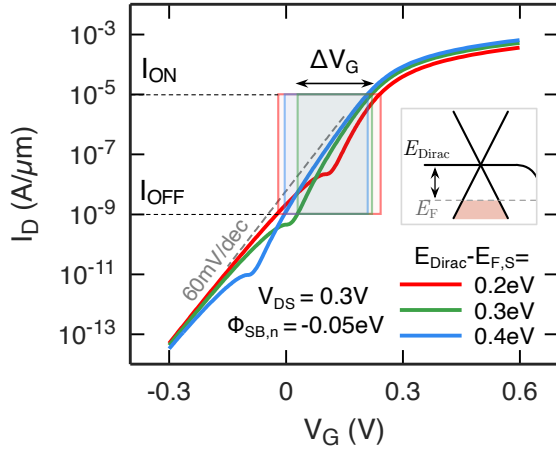


Fig. 3. Simulated transfer characteristics of an MoS₂ DS-FET with different doping levels in the graphene Dirac source.

steepest slope is achieved at a low current level below I_{OFF} and the SS above I_{OFF} is not as steep, which leads to a larger ΔV_G . On the other hand, for a too low doping level ($E_{Dirac}-E_{F,S} = 0.2$ eV, red line in Fig. 3), the kink is above I_{OFF} and the SS between the kink and I_{OFF} is above 60 mV/dec due to high-pass energy filtering above the Dirac point of graphene source, thus leading to a larger ΔV_G . Moreover, in the on-state, I_D at the same V_G for $E_{Dirac}-E_{F,S} = 0.2$ eV is decreased substantially compared with higher doping levels, since the E_{Dirac} is closer to $E_{F,S}$ and there are fewer modes in the graphene that contributes to the current conduction. Thus a large V_G is required to achieve the same I_{ON} , which leads to a further increase in ΔV_G . Only for an optimal doping level ($E_{Dirac}-E_{F,S} = 0.3$ eV, green line in Fig. 3), where the steepest SS is aligned with the target I_{OFF} , a lowest ΔV_G is achieved.

In summary, the doping level of graphene affects the position of the the kink in the $I_D - V_G$ characteristics, which is also the position of the steepest slope. Optimization of doping is essential to minimize ΔV_G of a DS-FET, which can be achieved by aligning the I_D of the kink with the target off-current I_{OFF} . We later adopt this technique in Section IV for benchmark of DS-FETs. Moreover, the correlation between the doping level of graphene and the current level of the steep SS is another signature of DS-FET operation, which should be examined in previous experimental demonstrations of 2D DS-FETs [13], [14] to validate the DS-FET operation.

B. Schottky Barrier Height

Next, we discuss the impact of the Schottky barrier height at the graphene-2DSC contact on the device performance of a 2D DS-FET. We show that a large Schottky barrier height not only leads to a lower on-state current, but may also degrades the SS.

In the previous simulations, we have assumed a negative Schottky barrier height [28] and a perfect transmission $T = 1$. However, for a positive Schottky barrier height, we need to consider the transmission of tunneling through a Schottky barrier, which can be calculated using Wentzel-Krammer-Brillouin (WKB) approximation [29], [30]:

$$T_{WKB}(E) = \exp\left(-2 \int_{x_s}^{x_e} \kappa(E) dx\right) \quad (7)$$

$$\kappa(E) = \frac{1}{\hbar} \sqrt{2m_e^* [E_C(x) - E]} \quad (8)$$

where x_s and x_e are the coordinates of the starting and ending points of the tunneling path, respectively, as shown in Fig. 4(a). With a larger Schottky barrier height, a lower transmission T leads to a lower on-current. Meanwhile, from eqs. (7) and (8), we can see that electrons with a higher energy tunnel through a

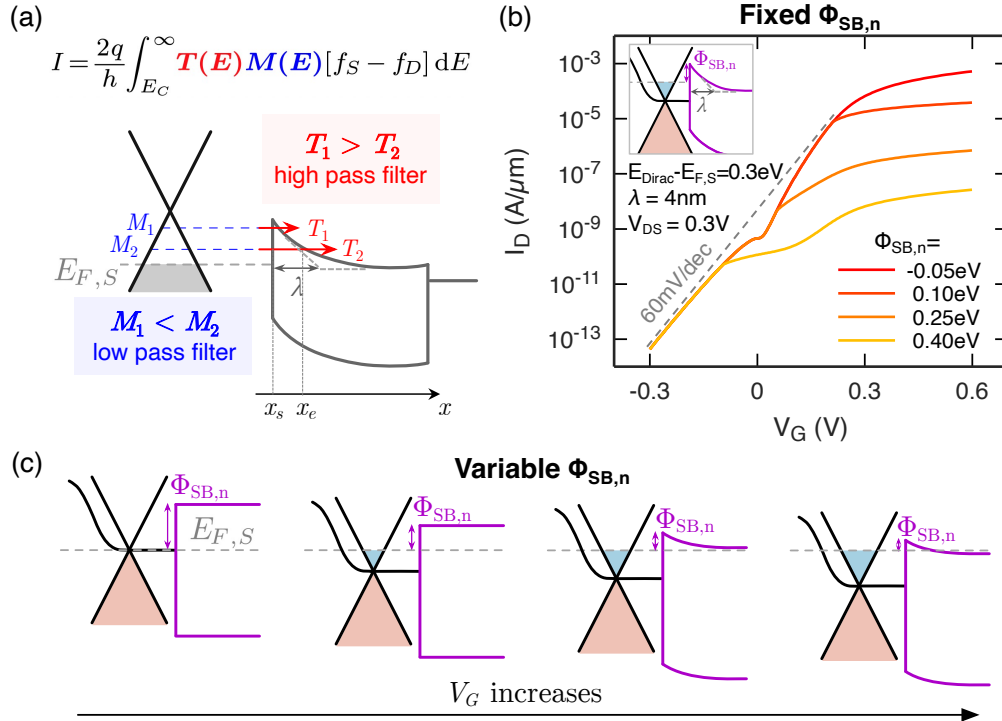


Fig. 4. (a) Illustration of Schottky barrier as a high pass filter. (b) Simulated transfer characteristics of an MoS₂ DS-FET with different Schottky barrier heights, assuming fixed Schottky barrier heights at graphene-MoS₂ contact. (c) Illustration of V_G -dependent Schottky barrier heights at graphene-MoS₂ contact.

thinner barrier and thus have a higher transmission, i.e. $T_1 > T_2$ for $E_1 > E_2$, as illustrated in Fig. 4(a). This indicates that the Schottky barrier tunneling acts as a high-pass filter and degrades the SS [31], [32], which works against the low-pass filter in the graphene Dirac source. Therefore, a large Schottky barrier height may affect the steep slope switching of a DS-FET.

Fig. 4(b) shows the simulated transfer characteristics of an MoS₂ DS-FET with different Schottky barrier heights for electrons, $\Phi_{SB,n}$. Note that in our device structure, since the gate G also covers a portion of the graphene that is in contact with the 2DSC channel [Fig. 1(a)], the Schottky barrier height is tuned by the gate voltage. Ignoring this effect for now, we have obtained the device characteristics as shown in Fig. 4(b). From Fig. 4(b), one can see that the on-current of the DS-FET decreases with a larger Schottky barrier height. Moreover, for a Schottky barrier height of 0.4 eV, the steep slope disappears because of the high-pass filtering effect of the large Schottky barrier.

According to Schottky-Mott rule [29], [33], the energy difference between the work function of undoped graphene (4.5 eV) and the electron affinity of MoS₂ (~4.1 eV) predicts a Schottky barrier height of ~0.4 eV. Thus, one may expect a degraded subthreshold slope for this device under any circumstances. However, as we mentioned before, the Schottky barrier height of the graphene-MoS₂ contact is tuned by the gate voltage. As illustrated in Fig. 4(c), at a small V_G , owing to the low DOS and thus the small C_q of graphene near the Dirac point, the band movement of graphene is almost one-to-one with V_G and is synchronized with that of MoS₂ [first and second panels in Fig. 4(c)]. Therefore, the Schottky barrier height decreases with increasing V_G and no triangular shaped barrier is formed, thus avoiding the degradation of SS. When V_G is further increased and E_F is further spaced from E_{Dirac} , the DOS of graphene becomes larger and the band movement of graphene slows down, and only then a triangular barrier is formed [third panel in Fig. 4(c)]. Therefore, the Schottky barrier at this point, is expected to be substantially lower than 0.4 eV and a less severe degradation of SS than shown in Fig. 4(b) for constant $\Phi_{SB,n}=0.4\text{eV}$ can be expected. For an even larger V_G , the Schottky barrier height continues to decrease when graphene

becomes more n-doped [fourth panel in Fig. 4(c)], and an improved I_{ON} is expected. In addition, previous experimental studies [16] and [17] have reported that even at zero gate voltage, the actual Schottky barrier height between graphene and MoS₂ is 100 to 150 meV, instead of 0.4 eV, due to charge transfer between graphene and MoS₂ upon contact, as indicated by DFT calculations [17].

In summary, for an MoS₂ DS-FET, an effective Schottky barrier height of ~100-150 meV is expected between the undoped graphene and MoS₂, which does not lead to a substantial degradation of the steep SS based on the simulation shown in Fig. 4(b); when the graphene is n-doped in the on-state ($V_G > 0$ V), the Schottky barrier height is further lowered by the n-type electrostatic doping of graphene, and an improved I_{ON} can be expected. However, for other 2D materials, especially those with lower electron affinities than MoS₂ (~4.1 eV), such as WS₂ (3.96 eV) and WSe₂ (3.65 eV) [34], one needs to carefully evaluate the Schottky barrier height at the graphene-2DSC contact [35] to avoid degradation of SS and I_{ON} of DS-FETs.

C. Effective Mass of Channel Material

Next, we discuss the impact of the effective mass of the channel material on the performance of 2D DS-FETs. In particular, we show that a too small effective mass leads to an incomplete energy filtering and thus a degradation in SS of a DS-FET, while a too large effective mass leads to a limited band movement in the on-state and thus a degradation in the on-state current I_{ON} .

We study an InAs nanosheet ($m_e^* = 0.023 m_0$, $g_C = 1$) and monolayer MoS₂ ($m_e^* = 0.51 m_0$, $g_C = 2$) as the respective examples of channel materials with small and large effective masses. Note that although InAs is typically considered a 3D material, there have been various reports on using ultra-thin InAs nanosheets for transistor applications [36], [37], and thus we can use the 2D DOS of the lowest subband of the InAs nanosheet for the calculation and treat it as a 2D material. Also note that the small bandgap of InAs ($E_g = 0.354$ eV) may induce a pronounced ambipolar hole injection from the drain side, thus impacting the off-state current [30], [38]. Yet, to simplify the discussion, we ignore the hole injection from the drain and

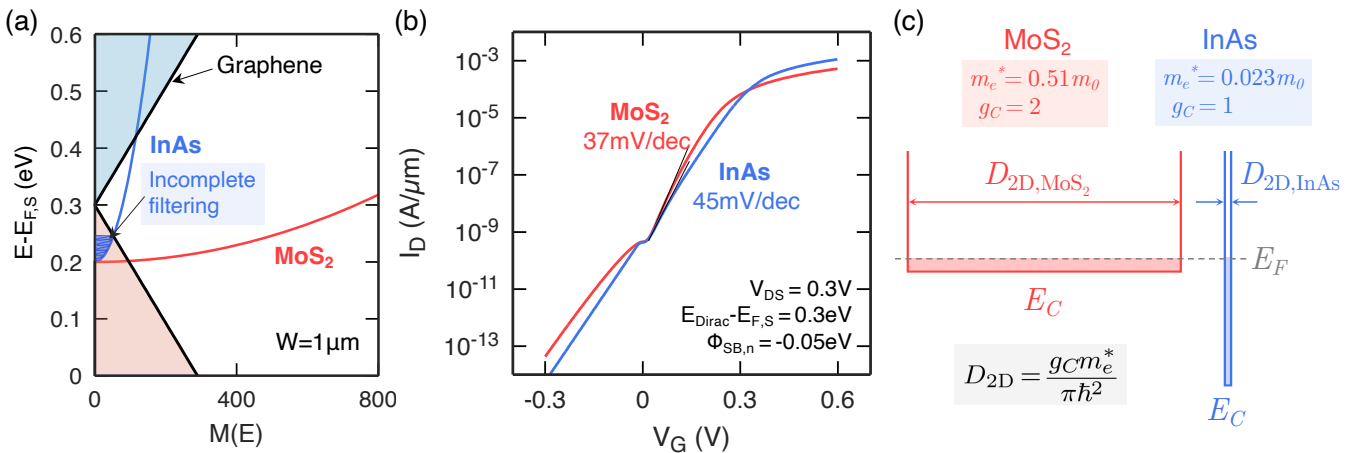


Fig. 5. (a) Number of modes in the graphene source, an InAs nanosheet and an MoS₂ channel, illustrating the incomplete filtering with an InAs channel. (b) Simulated transfer characteristics of MoS₂ and InAs DS-FETs. (c) Illustration of band movement in the ON-state in MoS₂ and InAs DS-FETs.

focus our discussion on the impact of the electron effective mass. Moreover, the quantization effect in the thickness direction leads to a larger bandgap of InAs nanosheets than its bulk value, thus alleviating the hole injection issue.

Fig. 5(a) shows the number of modes $M(E)$ of the graphene source (black line) and an InAs nanosheet channel (blue parabola), in comparison with $M(E)$ of an MoS₂ channel (red parabola). The InAs channel has a much lower $M(E)$ than the MoS₂ due to a much smaller effective mass ($m_e^* = 0.023 m_0$ vs. $m_e^* = 0.51 m_0$) and a smaller band degeneracy ($g_C = 1$ vs. $g_C = 2$). In an MoS₂ DS-FET, as we have discussed before, the number of modes is limited by the graphene Dirac source, and thus the low-pass energy filtering leads to a steep SS. However, in an InAs DS-FET, due to the smaller $M(E)$ of the InAs channel, the number of modes is limited by the $M(E)$ of InAs in the lower part of the energy window [the blue shaded region between the blue parabola and black line in Fig. 5(a)]. Therefore, since $M(E)$ does not decrease monotonically with higher energy E in the energy window, the low-pass filtering is incomplete, and thus a degradation of SS is expected.

Fig. 5(b) shows the simulated transfer characteristics of an InAs DS-FET and an MoS₂ DS-FET. One can see that the SS of the InAs DS-FET deteriorates to 45 mV/dec due to the incomplete energy filtering, compared to 37 mV/dec in the MoS₂ DS-FET. Therefore, at low gate voltages, the drain current I_D of the MoS₂ DS-FET is higher than that of the InAs DS-FET due to the steeper SS. However, at larger gate voltages, the drain current I_D of the InAs DS-FET surpasses that of the MoS₂ DS-FET. The lower I_{ON} of the MoS₂ DS-FET at larger gate voltages is the result of a limited band movement due to the larger effective mass of MoS₂. As illustrated in Fig. 5(c), the larger effective mass m_e^* (and larger band degeneracy g_C) leads to a larger 2D DOS D_{2D} (and thus a larger quantum capacitance C_q) for MoS₂. This in turn implies according to eqs. (5) and (6) that for the same gate voltage in the on-state, the conduction band E_C moves much less below E_F in case of MoS₂ than for InAs, as illustrated in Fig. 5(c). Therefore, the energy window for current conduction (roughly from E_C to E_F in the on state) is smaller in MoS₂, which leads to a degraded I_{ON} . Clearly, there is a V_{DD} dependence on which material is more favorable for higher I_{ON} , which will be discussed further in the ‘‘Benchmark’’ Section IV.

Moreover, DS-FETs are even more susceptible to I_{ON} degradation induced by large effective masses than MOSFETs. In conventional MOSFETs, the smaller energy window for a material with a large effective mass can be compensated by a larger number of modes $M(E)$, i.e., a larger integrand compensates for a smaller range of integration in the Landauer formula [eq. (1)]. However, in DS-FETs, since the graphene Dirac source is the bottleneck for $M(E)$, a material with a large effective mass does not benefit from a large $M(E)$, yet still suffers from a smaller energy window. Therefore, materials with large effective masses are at an even larger disadvantage in DS-FETs than in MOSFETs in terms of I_{ON} .

In summary, the effective mass of the channel material has a strong impact on the characteristics of a DS-FET. A too small effective mass leads to a degraded SS due to an incomplete low-pass filtering, while a too large effective mass leads to a degradation in I_{ON} due to a limited band movement in the on-

state, which is further worsened by the $M(E)$ bottleneck of the Dirac source. Therefore, there exists an optimal effective mass for DS-FETs, which we will further explore in the ‘‘Benchmark’’ Section IV.

D. Graphene Disorder

In the previous discussion, the graphene Dirac source is assumed to be disorder-free. However, it has been reported [39] that graphene is subject to random potential fluctuations caused by an inhomogeneous distribution of charged impurities in the substrate, leading to fluctuations of the Dirac point energy, as illustrated in Fig. 6(a). This effect, also known as ‘‘electron-hole puddles’’, results in a minimum conductivity of $4e^2/h$ of graphene [39]–[41], instead of the theoretical value of $4e^2/\pi h$ predicted by evanescent transport [42], a phenomenon often referred to as ‘‘the mystery of the missing π ’’. Next, we discuss the impact of such disorder on the performance of a 2D DS-FET.

Fig. 6(b) shows the number of modes in a disordered graphene source and an MoS₂ channel. We model the disorder as a fluctuation of the Dirac point energy that follows a Gaussian distribution with a variance $\sigma = 50$ meV [39] and assume that the number of modes is a superposition of the $M(E)$ across the distribution of Dirac point energies. Compared with the $M(E)$ in an ideal graphene in Fig. 1(c), $M(E)$ in a disordered graphene exhibits a non-zero value at the charge neutrality point, and thus the low-pass filtering effect is deteriorated. Fig. 6(c) shows the impact of the disorder on the transfer characteristics of an MoS₂ DS-FET. With a disordered graphene source, the SS of the DS-FET degrades to 47 mV/dec due to a deteriorated low-pass filtering effect, compared to 37 mV/dec with an ideal graphene source.

We would like to point out that the energy variance $\sigma = 50$ meV in ref. [39] was extracted when graphene is close to the charge neutrality point, where the DOS at the Fermi level is the lowest. However, in the p-doped graphene Dirac source of a n-type DS-FET, the DOS at $E_{F,S}$ (thus the quantum capacitance C_q) is larger than at the charge neutrality point. Since the origin of the disorder is the inhomogeneities of charged impurities on the substrate, the larger C_q results in a smaller fluctuation in E_{Dirac} , i.e., σ is expected to be lower than 50 meV in the p-doped graphene Dirac source, and thus the deterioration of SS is expected to be less severe than the prediction in Fig. 6(c). Moreover, since the length scale of the electron-hole puddles is ~ 30 nm [39], the impact of graphene disorder is further diminishing for DS-FETs with scaled dimensions.

Having discussed the performance degradation of a DS-FET due to an increased $M(E)$ close to the Dirac point that is caused by disorder, now we consider the performance improvement from a reduced $M(E)$ close to the Dirac point by introducing a bandgap in the graphene Dirac source, as illustrated in Fig. 6(d). A bandgap opening up to 250 meV has been reported in bilayer graphene by applying a vertical electric field [43], [44]. For simplicity, we assume an $E - k$ dispersion relation of:

$$E = E_{Dirac} \pm \hbar v_F \sqrt{k^2 + (E_{g,DS}/2)^2} \quad (9)$$

for the gapped Dirac source, where $E_{g,DS}$ is the bandgap. $M(E)$ of the gapped graphene is calculated as:

the DS-FET [Fig. 1(a)], which serves to lower the Schottky barrier height between graphene and 2DSC. Since the cold electrons injected from the p-type graphene source are not in thermal equilibrium with the n-type graphene, inelastic scattering in the n-doped graphene segment will destroy the $M(E)$ information carried over from the cold electron source and rethermalize the electrons [45], [46]. In the worst case scenario, the electron distribution is rethermalized to a room-temperature (RT) distribution, and the SS of the DS-FET goes back to 60 mV/dec (or even worse, considering the high-pass filtering effect of the n-doped graphene).

To prevent the SS degradation induced by rethermalization, the length of the n-doped graphene segment should be short enough to minimize the scattering. Note that only inelastic scattering, such as phonon scattering, leads to rethermalization, while elastic scattering, such as charged impurity scattering, only changes the electron momentum but does not alter the energy spectrum, thus not contributing to rethermalization. Therefore, the length of the n-doped graphene segment, i.e., the critical length scale for rethermalization L_{crit} , should be much smaller than the mean free path associated with phonon scattering, λ_{phonon} , instead of the mean free path that accounts for all scattering events. A previous paper [47] has mapped out the electron mean free paths in graphene using scanning capacitance microscopy and analyzed the individual contributions to the mean free path from different scattering

mechanisms, including resonant scatterers (RS), charged impurities (CI) and surface polar phonons (SPP). It was determined that the mean free path associated with SPP scattering is around 300 nm to 1 μm , depending on the substrate properties, such as permittivity [48]. Interestingly, previously demonstrated MoS₂ DS-FETs [13], [14] have rather long (5-10 μm) graphene-MoS₂ contact lengths. In light of the expected rethermalization described here, the occurrence of steep slopes in these devices is unexpected and should be carefully revisited to better understand their origin.

IV. BENCHMARK

In this section, we discuss the benchmark of channel materials for 2D DS-FETs. We adopt a similar benchmarking methodology as in ref. [5], i.e., fixing an I_{OFF} target and comparing the I_{ON} for a given V_{DD} . The detailed procedures for the benchmarking effort, as illustrated in Fig. 8(a), is as follows:

- i) Select the optimal doping level of the graphene Dirac source for a given I_{OFF} target, i.e., align the kink in the $I_D - V_G$ characteristics with I_{OFF} ;
- ii) Shift the kink to $V_G = 0$ V (in real devices, this can be achieved with a proper V_{th} tuning);
- iii) Determine the I_{ON} , i.e., I_D at $V_G = V_{\text{DD}}$.

For simplicity, we only consider the differences in electron effective mass m_e^* and conduction band valley degeneracy g_c for different channel materials in the benchmark, and assume

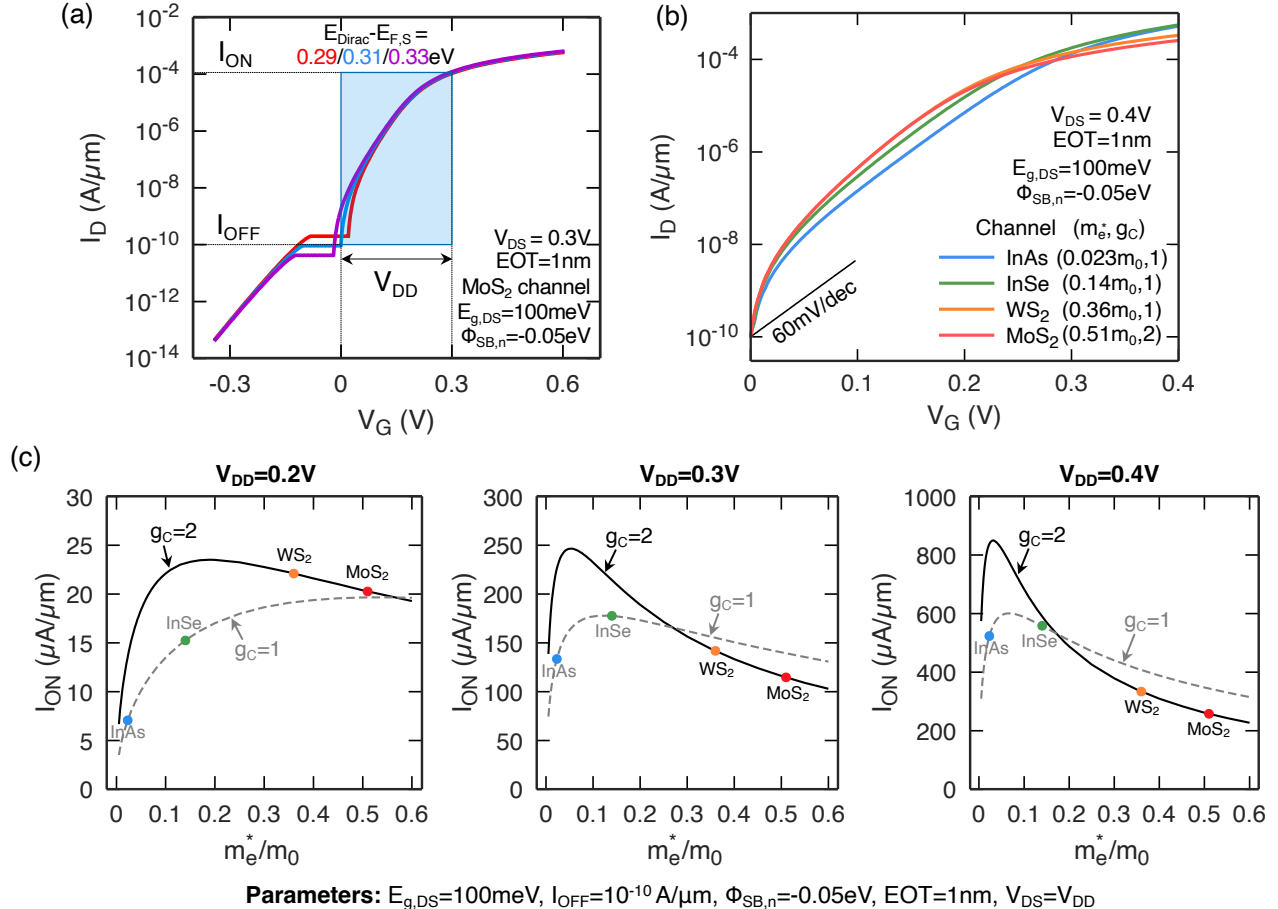


Fig. 8. (a) Illustration of the benchmarking methodology. (b) Simulated transfer characteristics of DS-FETs with different channel materials. (c) Benchmark of DS-FETs with different channel materials for $V_{\text{DD}} = 0.2$ V, 0.3V and 0.4 V.

other parameters to be the same, such as Schottky barrier height at the graphene-2DSC contact and EOT of the gate oxide, although these parameters can be material-dependent in real devices. Also, as in Section III-C, we ignore any potentially existing the ambipolar injection from the drain side.

Fig. 8(b) shows the simulated transfer characteristics of DS-FETs for four different channel materials after doping level optimization and V_{th} shifting: (a) InAs ($m_e^* = 0.023 m_0$, $g_C = 1$); (b) InSe ($m_e^* = 0.14 m_0$, $g_C = 1$) [49]; (c) WS₂ ($m_e^* = 0.36 m_0$, $g_C = 2$) [50]; (d) MoS₂ ($m_e^* = 0.51 m_0$, $g_C = 2$) [22]. An I_{OFF} target of 10^{-10} A/ μm is selected and a gapped graphene Dirac source with $E_{g,DS} = 100$ meV is used. As we have discussed in Section III-C, InAs and InSe DS-FETs exhibit degraded SS due to an incomplete low-pass filtering. Interestingly, even the on-currents are lower than for WS₂ and MoS₂ DS-FETs at $V_G = 0.2$ V because the devices are still deep in the off-state for this voltage. However, at higher V_G , because of the larger energy window for conduction with a smaller effective mass and band degeneracy, I_{ON} of InAs and InSe DS-FETs surpass I_{ON} of WS₂ and MoS₂ DS-FETs, with a crossover at around $V_G = 0.25$ V.

Fig. 8(c) shows the benchmark results, in terms of I_{ON} as a function of effective mass of channel material, for DS-FETs at different supply voltages V_{DD} . For $V_{DD} = 0.2$ V, the peak I_{ON} is achieved at $m_e^* \sim 0.18 m_0$ and $g_C = 2$, and WS₂ has the best performance of the four materials under consideration, while InAs has the worst because of the SS degradation. For $V_{DD} = 0.3$ V, the peak I_{ON} is achieved at $m_e^* \sim 0.05 m_0$ and $g_C = 2$, and of the four materials under study, InSe has the highest I_{ON} , while MoS₂ has a lowest I_{ON} due to a limited band movement. For $V_{DD} = 0.4$ V, the peak I_{ON} is achieved at $m_e^* \sim 0.025 m_0$ and $g_C = 2$, and of the four materials that are evaluated here, InSe has the best performance, and InAs comes as a close second, while MoS₂ again has the worst performance due to a limited band movement in the on-state. The general trend is that at a low V_{DD} , channel materials with a moderate m_e^* that is not too small to exhibit SS degradation, nor too large to be limited in band movement, are more favorable for highest performance; while at a high V_{DD} , the optimal m_e^* shifts to an even smaller value of m_e^* for which SS degradation is already present, since the advantage of a larger band movement overcomes the disadvantage of a worse SS.

Finally, it is worth noticing that some factors have been ignored for convenience in our benchmarking, which may be important and should be taken into account for real applications. For example, while WS₂ outperforms MoS₂ at all V_{DD} values in Fig. 8(c), the Schottky barrier height between graphene and WS₂ is expected to be larger than for MoS₂, which may degrade the performance. Another example is that the small bandgap of InAs ($E_g = 0.354$ eV) may cause ambipolar injection from the drain and lead to a degradation of I_{OFF} , which we have ignored in the discussion.

V. CONCLUSION

In this paper, we have discussed various design considerations of 2D DS-FETs. The basic operation principles of 2D DS-FETs are introduced, followed by a discussion on the impact of device parameters and non-idealities on the performance of 2D DS-FETs. Finally, we have benchmarked the performance of DS-FETs from different channel materials,

such as InAs, InSe, WS₂ and MoS₂. Our study provides guidance for the design of 2D DS-FETs.

REFERENCES

- [1] H. Lu and A. Seabaugh, "Tunnel field-effect transistors: State-of-the-art," *IEEE J. Electron Devices Soc.*, vol. 2, no. 4, pp. 44–49, 2014, doi: 10.1109/JEDS.2014.2326622.
- [2] J. Appenzeller, Y.-M. Lin, J. Knoch, and P. Avouris, "Band-to-Band Tunneling in Carbon Nanotube Field-Effect Transistors," *Phys. Rev. Lett.*, vol. 93, no. 19, p. 196805, Nov. 2004, doi: 10.1103/PhysRevLett.93.196805.
- [3] J. Appenzeller, Y.-M. Lin, J. Knoch, Z. Chen, and P. Avouris, "Comparing Carbon Nanotube Transistors—The Ideal Choice: A Novel Tunneling Device Design," *IEEE Trans. Electron Devices*, vol. 52, no. 12, pp. 2568–2576, Dec. 2005, doi: 10.1109/TED.2005.859654.
- [4] E. Memisevic, J. Svensson, M. Hellenbrand, E. Lind, and L.-E. Wernersson, "Vertical InAs/GaAsSb/GaSb tunneling field-effect transistor on Si with $S = 48$ mV/decade and $I_{on} = 10$ $\mu\text{A}/\mu\text{m}$ for $I_{off} = 1$ nA/ μm at $V_{ds} = 0.3$ V," in *2016 IEEE International Electron Devices Meeting (IEDM)*, Dec. 2016, pp. 19.1.1-19.1.4, doi: 10.1109/IEDM.2016.7838450.
- [5] U. E. Avci, D. H. Morris, and I. A. Young, "Tunnel Field-Effect Transistors: Prospects and Challenges," *IEEE J. Electron Devices Soc.*, vol. 3, no. 3, pp. 88–95, May 2015, doi: 10.1109/JEDS.2015.2390591.
- [6] S. Salahuddin and S. Datta, "Use of negative capacitance to provide voltage amplification for low power nanoscale devices," *Nano Lett.*, vol. 8, no. 2, pp. 405–410, 2008, doi: 10.1021/nl071804g.
- [7] W. Cao and K. Banerjee, "Is negative capacitance FET a steep-slope logic switch?," *Nat. Commun.*, vol. 11, no. 1, 2020, doi: 10.1038/s41467-019-13797-9.
- [8] H. Kam, V. Pott, R. Nathanael, Jaeseok Jeon, Elad Alon, and Tsu-Jae King Liu, "Design and reliability of a micro-relay technology for zero-standby-power digital logic applications," in *2009 IEEE International Electron Devices Meeting (IEDM)*, Dec. 2009, pp. 1–4, doi: 10.1109/IEDM.2009.5424218.
- [9] K. Gopalakrishnan, P. B. Griffin, and J. D. Plummer, "I-MOS: a novel semiconductor device with a subthreshold slope lower than kT/q ," in *Digest. International Electron Devices Meeting*, 2002, pp. 289–292, doi: 10.1109/IEDM.2002.1175835.
- [10] K. Gopalakrishnan, P. B. Griffin, and J. D. Plummer, "Impact Ionization MOS (I-MOS)—Part I: Device and Circuit Simulations," *IEEE Trans. Electron Devices*, vol. 52, no. 1, pp. 69–76, Jan. 2005, doi: 10.1109/TED.2004.841344.
- [11] C. Qiu *et al.*, "Dirac-source field-effect transistors as energy-efficient, high-performance electronic switches," *Science*, vol. 361, no. 6400, pp. 387–392, Jul. 2018, doi: 10.1126/science.aap9195.
- [12] F. Liu, C. Qiu, Z. Zhang, L.-M. Peng, J. Wang, and H. Guo, "Dirac Electrons at the Source: Breaking the 60-mV/Decade Switching Limit," *IEEE Trans. Electron Devices*, vol. 65, no. 7, pp. 2736–2743, Jul. 2018, doi: 10.1109/TED.2018.2836387.
- [13] M. Liu *et al.*, "Monolayer MoS₂ Steep-slope Transistors with Record-high Sub-60-mV/decade Current Density Using Dirac-source Electron Injection," in *2020 IEEE International Electron Devices Meeting (IEDM)*, Dec. 2020, pp. 12.5.1-12.5.4, doi: 10.1109/IEDM13553.2020.9371961.
- [14] Z. Tang *et al.*, "A Steep-Slope MoS₂/Graphene Dirac-Source Field-Effect Transistor with a Large Drive Current," *Nano Lett.*, vol. 21, no. 4, pp. 1758–1764, Feb. 2021, doi: 10.1021/acs.nanolett.0c04657.
- [15] H. Yang *et al.*, "Graphene barristor, a triode device with a gate-controlled Schottky barrier," *Science*, vol. 336, no. 6085, pp. 1140–1143, 2012, doi: 10.1126/science.1220527.
- [16] W. J. Yu *et al.*, "Vertically stacked multi-heterostructures of layered materials for logic transistors and complementary inverters," *Nat. Mater.*, vol. 12, no. 3, pp. 246–252, 2013, doi: 10.1038/nmat3518.
- [17] L. Yu *et al.*, "Graphene/MoS₂ Hybrid technology for large-scale two-dimensional electronics," *Nano Lett.*, vol. 14, no. 6, pp. 3055–3063, 2014, doi: 10.1021/nl404795z.
- [18] C.-H. Yeh, W. Cao, A. Pal, K. Parto, and K. Banerjee, "Area-Selective-CVD Technology Enabled Top-Gated and Scalable 2D-Heterojunction Transistors with Dynamically Tunable Schottky Barrier," in *2019 IEEE International Electron Devices Meeting (IEDM)*, Dec. 2019, pp. 23.4.1-23.4.4, doi: 10.1109/IEDM19573.2019.8993600.

- [19] R. Landauer, "Spatial Variation of Currents and Fields Due to Localized Scatterers in Metallic Conduction," *IBM J. Res. Dev.*, vol. 1, no. 3, pp. 223–231, Jul. 1957, doi: 10.1147/rd.13.0223.
- [20] S. Datta, *Electronic Transport in Mesoscopic Systems*. Cambridge University Press, 1995.
- [21] M. Lundstrom, *Fundamentals of Carrier Transport*. Cambridge University Press, 2000.
- [22] Z. Jin, X. Li, J. T. Mullen, and K. W. Kim, "Intrinsic transport properties of electrons and holes in monolayer transition-metal dichalcogenides," *Phys. Rev. B*, vol. 90, no. 4, p. 045422, Jul. 2014, doi: 10.1103/PhysRevB.90.045422.
- [23] K. F. Mak, C. Lee, J. Hone, J. Shan, and T. F. Heinz, "Atomically Thin MoS₂: A New Direct-Gap Semiconductor," *Phys. Rev. Lett.*, vol. 105, no. 13, p. 136805, Sep. 2010, doi: 10.1103/PhysRevLett.105.136805.
- [24] M. I. Katsnelson, K. S. Novoselov, and A. K. Geim, "Chiral tunnelling and the Klein paradox in graphene," *Nat. Phys.*, vol. 2, no. 9, pp. 620–625, Sep. 2006, doi: 10.1038/nphys384.
- [25] C. W. J. Beenakker, "Colloquium: Andreev reflection and Klein tunneling in graphene," *Rev. Mod. Phys.*, vol. 80, no. 4, pp. 1337–1354, Oct. 2008, doi: 10.1103/RevModPhys.80.1337.
- [26] D. L. John, L. C. Castro, and D. L. Pulfrey, "Quantum capacitance in nanoscale device modeling," *J. Appl. Phys.*, vol. 96, no. 9, pp. 5180–5184, Nov. 2004, doi: 10.1063/1.1803614.
- [27] A. Rahman, Jing Guo, S. Datta, and M. S. Lundstrom, "Theory of ballistic nanotransistors," *IEEE Trans. Electron Devices*, vol. 50, no. 9, pp. 1853–1864, Sep. 2003, doi: 10.1109/TED.2003.815366.
- [28] Jing Guo and M. S. Lundstrom, "A computational study of thin-body, double-gate, Schottky barrier MOSFETs," *IEEE Trans. Electron Devices*, vol. 49, no. 11, pp. 1897–1902, Nov. 2002, doi: 10.1109/TED.2002.804696.
- [29] S. M. Sze and K. K. Ng, *Physics of Semiconductor Devices*. Hoboken, NJ, USA: John Wiley & Sons, Inc., 2006.
- [30] A. V. Penumatcha, R. B. Salazar, and J. Appenzeller, "Analysing black phosphorus transistors using an analytic Schottky barrier MOSFET model," *Nat. Commun.*, vol. 6, p. 8948, 2015, doi: 10.1038/ncomms9948.
- [31] P. M. Solomon, "Inability of Single Carrier Tunneling Barriers to Give Subthermal Subthreshold Swings in MOSFETs," *IEEE Electron Device Lett.*, vol. 31, no. 6, pp. 618–620, Jun. 2010, doi: 10.1109/LED.2010.2046713.
- [32] J. Appenzeller, F. Zhang, S. Das, and J. Knoch, "Transition metal dichalcogenide schottky barrier transistors: A device analysis and material comparison," in *2D Materials for Nanoelectronics*, 2016.
- [33] Y. Liu *et al.*, "Approaching the Schottky–Mott limit in van der Waals metal–semiconductor junctions," *Nature*, vol. 557, no. 7707, pp. 696–700, May 2018, doi: 10.1038/s41586-018-0129-8.
- [34] H. Kim and H. J. Choi, "Thickness dependence of work function, ionization energy, and electron affinity of Mo and W dichalcogenides from DFT and GW calculations," *Phys. Rev. B*, vol. 103, no. 8, p. 085404, Feb. 2021, doi: 10.1103/PhysRevB.103.085404.
- [35] K. Kim *et al.*, "Band alignment in WSe₂-graphene heterostructures," *ACS Nano*, 2015, doi: 10.1021/acsnano.5b01114.
- [36] H. Ko *et al.*, "Ultrathin compound semiconductor on insulator layers for high-performance nanoscale transistors," *Nature*, vol. 468, no. 7321, pp. 286–289, Nov. 2010, doi: 10.1038/nature09541.
- [37] J. Nah *et al.*, "III–V Complementary Metal–Oxide–Semiconductor Electronics on Silicon Substrates," *Nano Lett.*, vol. 12, no. 7, pp. 3592–3595, Jul. 2012, doi: 10.1021/nl301254z.
- [38] P. Wu and J. Appenzeller, "Toward CMOS like devices from two-dimensional channel materials," *APL Mater.*, vol. 7, no. 10, p. 100701, Oct. 2019, doi: 10.1063/1.5115147.
- [39] J. Martin *et al.*, "Observation of electron–hole puddles in graphene using a scanning single-electron transistor," *Nat. Phys.*, vol. 4, no. 2, pp. 144–148, Feb. 2008, doi: 10.1038/nphys781.
- [40] K. S. Novoselov *et al.*, "Two-dimensional gas of massless Dirac fermions in graphene," *Nature*, vol. 438, no. 7065, pp. 197–200, Nov. 2005, doi: 10.1038/nature04233.
- [41] Y. Sui, T. Low, M. Lundstrom, and J. Appenzeller, "Signatures of Disorder in the Minimum Conductivity of Graphene," *Nano Lett.*, vol. 11, no. 3, pp. 1319–1322, Mar. 2011, doi: 10.1021/nl104399z.
- [42] M. I. Katsnelson, "Zitterbewegung, chirality, and minimal conductivity in graphene," *Eur. Phys. J. B*, vol. 51, no. 2, pp. 157–160, May 2006, doi: 10.1140/epjb/e2006-00203-1.
- [43] Y. Zhang *et al.*, "Direct observation of a widely tunable bandgap in bilayer graphene," *Nature*, vol. 459, no. 7248, pp. 820–823, Jun. 2009, doi: 10.1038/nature08105.
- [44] T. Chu and Z. Chen, "Achieving large transport bandgaps in bilayer graphene," *Nano Res.*, vol. 8, no. 10, pp. 3228–3236, Oct. 2015, doi: 10.1007/s12274-015-0823-x.
- [45] W. Gan *et al.*, "Design and Simulation of Steep-Slope Silicon Cold Source FETs With Effective Carrier Distribution Model," *IEEE Trans. Electron Devices*, vol. 67, no. 6, pp. 2243–2248, Jun. 2020, doi: 10.1109/TED.2020.2988855.
- [46] E. A. A. Pogna *et al.*, "Hot-Carrier Cooling in High-Quality Graphene Is Intrinsically Limited by Optical Phonons," *ACS Nano*, vol. 15, no. 7, pp. 11285–11295, Jul. 2021, doi: 10.1021/acsnano.0c10864.
- [47] F. Giannazzo, S. Sonde, R. Lo Nigro, E. Rimini, and V. Raineri, "Mapping the Density of Scattering Centers Limiting the Electron Mean Free Path in Graphene," *Nano Lett.*, vol. 11, no. 11, pp. 4612–4618, Nov. 2011, doi: 10.1021/nl2020922.
- [48] V. Perebeinos and P. Avouris, "Inelastic scattering and current saturation in graphene," *Phys. Rev. B*, vol. 81, no. 19, p. 195442, May 2010, doi: 10.1103/PhysRevB.81.195442.
- [49] D. A. Bandurin *et al.*, "High electron mobility, quantum Hall effect and anomalous optical response in atomically thin InSe," *Nat. Nanotechnol.*, vol. 12, no. 3, pp. 223–227, Mar. 2017, doi: 10.1038/nnano.2016.242.
- [50] G. Gaddemane, S. Gopalan, M. L. Van de Put, and M. V. Fischetti, "Limitations of ab initio methods to predict the electronic-transport properties of two-dimensional semiconductors: the computational example of 2H-phase transition metal dichalcogenides," *J. Comput. Electron.*, vol. 20, no. 1, pp. 49–59, Feb. 2021, doi: 10.1007/s10825-020-01526-1.